HUNGARIAN JOURNAL OF
INDUSTRY AND CHEMISTRY
Vol. 52(2) pp. 47–56 (2024)
hjic.mk.uni-pannon.hu
DOI: 10.33927/hjic-2024-18

HOW TO AVOID ACID CORROSION OF LAMINATED SOLAR PANELS BY REPLACING THE ENCAPSULANT

GERGELY BALÁZS PATTHY[1], MÁRTON SZIGETI[2], ZSÓFIA ZÁVODI-FODOR[3], MÁTYÁS VASÁROS[3] AND MIKLÓS JAKAB[1]*

1 Department of Materials Engineering, Research Centre for Engineering Sciences, University of Pannonia, Egyetem u. 10, Veszprém, 8200, HUNGARY
2 Research Group of Corrosion, University of Pannonia, Egyetem u. 10, Veszprém, 8200, HUNGARY
3 CoreComm SI Ltd., Lőpor körút 9, Veszprém, 8200, HUNGARY

Solar power is gaining more and more importance in terms of electricity generation worldwide. As the solar industry today is still linear (the majority of the panel waste is not recycled), ensuring a long lifetime of the panels is important. Today, the most commonly used encapsulant is ethylene-vinyl acetate (EVA), a copolymer prominent since the 1980's. However, as this material ages, it releases acetic acid, which is highly corrosive. As a result, alternatives to EVA are required. In this paper, a prospective alternative, a polyethylene-based elastomer-type foil, namely a polyolefin elastomer (POE), is investigated and compared to EVA from a corrosion point of view. Firstly, the two raw materials are compared on the basis of their chemical composition and thermal stability. Both foils are used to manufacture a batch of standard solar panels, which are then subjected to a standardized climate chamber test. During and after these tests, the power generated by the solar panels is monitored and the state of the wafers examined by an electroluminescence test. Furthermore, the effect of the free acetic acid is examined in a corrosion model test, where the subjected wafers are compared in a before-and-after microscopic examination.

Keywords: solar panels, EVA, EVA alternatives, Solar POE, acetic acid corrosion

1. Introduction

Over recent years, solar power has gained significant importance. According to the International Energy Agency (IEA), the total amount of electricity generated by this means was 825 700 GWh globally in 2020, a 25.8 times increase compared to 2010, where this value was just 32 004 GWh, moreover, further growth is anticipated [1]. Because of its growing significance, the reliability and longevity of solar panels must be ensured.

The actual lifetime of solar panels, however, is difficult to predict as their ageing and failure modes are not only dependent on the materials used and manufacturing technique but also on the climate as well as where and how they were installed (the latter is not only important from a corrosion and degradation point of view but also in terms of energetics) [2]-[3]. During their lifetime, solar cells must endure the degrading effects of weather such as temperature fluctuations, moisture originating from rain and humidity, UV radiation as well as different mechanical forces such as the wind or snow. These forces degrade the solar panels and eventually lead to their total failure. In a survey conducted by the IEA, it was revealed that the most common failure modes in the climate category 'moderate' were Potential Induced Corrosion/Degradation (PID for short) and delamination [3]. According to multiple works, PID is a special corrosion phenomenon caused mostly by the polarizing effect of sunlight (but other electrochemical routes are also known). It is a localized corrosion method where conducting ions and the polarizing light induce a current between the wafers and the ground as the cell matrix will have a more negative potential when compared to the ground. The rate of corrosion is dependent on numerous factors, e.g. the potential of the cell measured regarding the ground as well as the structure and materials of the cell [4]-[5]. According to Hasan et al., the local negative potential is mainly caused by the free sodium ions, which leave the glass in an ion exchange/glass corrosion mechanism. This local buildup of ions is conductive and because of the severe corrosion it causes the PID irreversibly damages the affected area. This effect is almost always accompanied by delamination, which could originate from the degradation and decomposition of the encapsulant [6].

As an encapsulant, one material stands out in the industry, namely ethylene-vinyl acetate (EVA). This

Received: 6 June 2024; Revised: 9 Aug 2024;
Accepted: 9 Aug 2024
*Correspondence: jakab.miklos@mk.uni-pannon.hu

copolymer has outstanding qualities: if it is baked correctly in a vacuum furnace, the final product becomes entirely transparent and creates a strong bonding force both with the other base materials and with itself, making it suitable for lamination techniques. As a result, it is suitable as a mechanical coupler as well as an electrical and thermal insulator, while letting light into the wafers [3, 6-7].

These qualities have rendered EVA the dominant encapsulating-binding agent in the solar power industry since the 1980's. However, later studies found mechanisms and qualities that made the use of this material questionable [6, 8-9].

The degradation of the polymer has been described by Marín et al., who even described the kinetic model of decomposition. However, only the high-temperature thermal degradation of EVA was taken into account, which was observed by thermogravimetric analysis between 530 and 560 K. This revealed a really detrimental mechanism: the main decomposition product of which was found to be acetic acid [10].

Later works also investigated the degradation of EVA at lower temperatures. Under normal operating conditions, the effects of decomposition and corrosion still occur [11]-[13].

Decomposition of the EVA foil is the result of a thermal and photo-induced series of reactions which can be categorized into two parts: the formation of an organic oxo compound, which is typically an aldehyde or acid, resulting from Norrish reactions. The other subcategory consists of the further oxidation of the remaining polymer chain as a result of environmental oxygen, typically the oxidation of polyene.

The Norrish reactions can be further divided into three subcategories. These reactions are in the form of the UV-induced decomposition of radicals and can be seen in *Figure 1*. In the first Norrish reaction, an acetocarbonyl radical leaves the main chain before reacting with another molecule with free hydrogen atoms, leaving behind acetaldehyde, methane, carbon dioxide or carbon monoxide, depending on the other molecule. The second Norrish reaction is the most significant one whereby a whole acetic acid molecule leaves the polymer chain resulting in a polyene molecule and acetic acid. This reaction causes the discoloration of EVA and a free corrosive to form in the solar panel. The third Norrish reaction is very similar to the first, however, the resulting products are acetaldehyde and a ketone [14]-[15].

Further oxidation of the polymer chain usually produces α,β-unsaturated carbonyl compounds. After the formation of acetic acid as a result of a second Norrish reaction, an oxygen molecule binds to the remaining polymer chain, essentially creating a hydroperoxide. Next a water molecule leaves the chain to produce a carbonyl (ketone)-type molecule, resulting in a diluted aqueous solution of acetic acid [15]. The yield of this second Norrish reaction can be high. In one experiment, Miller et al. found that at higher operating temperatures, more acid is produced, e.g. a 50 mg sample held at 80 °C for 526 days yielded 176 ng of acetic acid [16].

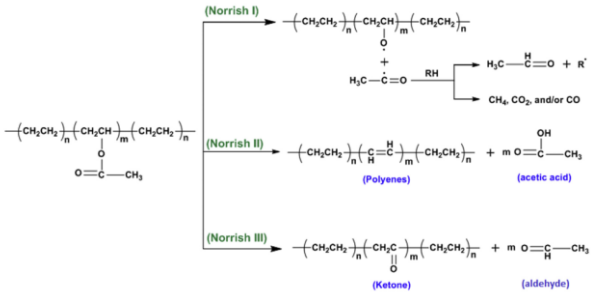

Figure 1: The decomposition routes of EVA [14]

For this reason, other additives, mainly UV absorbers and antioxidants, were introduced in the polymer to enhance its degradation resistance [14]-[15].

Despite these efforts, these materials only delayed the degradation of the encapsulant and could not stop the production of acetic acid. As this chemical causes severe corrosion in the solar panel (both direct acidic corrosion and while reacting with the glass as the result of an ion exchange mechanism, PID), other materials are also used in the industry [12-13, 17-18]. Most alternative materials for encapsulants, e.g. polyurethanes or epoxy resins, are not used extensively. However, other groups are promising, that is, the so-called thermoplastic polyolefins (TPO) and polyolefin elastomers (POE). These materials can be crosslinking or non-crosslinking, the latter can even eliminate the problems associated with peroxide-induced crosslinking mechanisms. The main goal of this development is to achieve properties as close as possible to those of EVA without the negative mechanisms associated with it. Moreover, future solar panels should be easier to recycle than those currently produced, as the economic structure of solar panels is currently linear and the aim would be to make them circular [7, 14, 17, 19-20]. One such elastomer is the subject of this paper, which is examined from a corrosion and degradation standpoint.

The goal of this article is to compare the degradation and aging effects of the two types of plastic encapsulants. First, the exact composition of the foils is determined. Artificial aging of the factory-assembled panels is achieved by treating the cells in a climate chamber which has a standardized temperature curve [21]-[22]. The solar panels were subjected to a handful of measurements to precisely determine the outcome of the treatment. During the research, the effects of acetic acid on the wafers was also investigated to understand the severity and mechanisms of degradation of these components.

2. Experimental

2.1. Manufacturing process of the examined solar panels

The solar panels are made with a laminated object manufacturing technology by our industrial partner. In accordance with the secrecy agreements, the names of the

Table 1: The layers of the solar panels

Layer		Thickness (mm)
1	Glass (tempered, soda lime)	3.2
2	EVA/POE foil	0.2
3	Cell Matrix assembly (wafers and ribbons)	0.5
4	EVA/POE foil	0.2
5	Isotactic PP backsheet	0.2

products and parameters of lamination are considered insider know-how data and have been omitted from this paper.

The main components of the cells are the wafers. These are standard anti-glare monocrystalline silicon solar wafers. With dimensions of 156 mm x 156 mm, they are manufactured in China, one-way doped with phosphorus (n-type) at an illumination level of 1000 W/m^2 yielding a power of 5 W at 0.5 V and 10 A. Using a laser cutting machine, the wafer is cut into smaller pieces to prevent loss in electrical power as the magnitude of the current is proportional to the surface area of the wafer. To prevent having a negative effect on the depleted zone if cut through, the laser cutter only scratches the surface, the cutting is finished manually. These pieces are then ordered according to polarity and sent to an automatic soldering line, where they are soldered in series, creating the basic unit of electricity generation, the strings. The connecting material is called ribbon, which is sourced from China and is made of a copper wire coated with a lead-based solder consisting of ~60 wt.% tin and ~40 wt.% lead fluxed externally. After this step, the assembly of the solar panel begins by hand on a multi-station production line. These stations are connected by a Bosch transfer system. Firstly, a glass pane is put into the jig which acts as the main carrier material. It is construction-grade, thermally tempered soda-lime glass manufactured in China. The glass pane is cleaned with isopropyl alcohol manufactured in Hungary before the first layer of binding-insulating foil is laid onto it. The foil is often an EVA foil sourced from China, that is, a copolymer consisting of 72 wt.% ethylene and 28 wt.% vinyl acetate. POE can also be used here, which is composed of polyethylene and a small amount of polyamide according to the Chinese manufacturer's datasheet. After the layering step, the operators inserted two strips of polytetrafluoroethylene (PTFE) to protect the glass and the foil during the soldering step. The strings are then arranged in accordance with their polarity by a special jig. The strings are fixed in place by applying a small amount of heat to the back of the wafers, making the binding foil adhere to them. The strings are then soldered together with ribbons on one side which contains Schottky diodes that isolate the string from the cell matrix while not under a sufficient level of illumination. Next a layer of glass foil to ensure that the strings remain still while the lamination process is ongoing, a layer of binding foil and the backsheet are inserted. The backsheet is made of black and white-colored isotactic polypropylene manufactured in India. After a quick inspection and voltage test, the cell is placed on the conveyor belt of the oil vacuum laminator where it is heated under vacuum for about 600 seconds at ~160 °C. After the treatment, the panel is left to cool down and the excess plastic cut off. The layers and their thicknesses are summarized in *Table 1*.

2.2. Testing methods

As corrosion resistance is directly related to the materials used in the manufacturing process, examination of both the materials and final solar panel was deemed necessary to obtain both chemical and physical information from the samples and base materials. In order to obtain these data, Fourier-transform infrared spectroscopy (FTIR), differential scanning calorimetry (DSC), gel content test and energy dispersive X-ray spectroscopy (EDS) methods were used. The stability of the binding foil in its final state can be predicted by the gel content test. The product was subjected to a climate chamber test to simulate the effects of weather on the solar panels. These effects were examined by a power measurement and electroluminescence (EL) test. The materials were subjected to a corrosion model test to simulate decomposition of the EVA foil, the effects of which were observable by microscopic methods.

Fourier-transform infrared spectroscopy (FTIR)

FTIR was used to determine the exact composition of the used plastic materials by irradiating the sample with infrared light and detecting the level of absorbance at that particular wavelength. The method used a narrow spectrum (non-monochromatic) light source to collect data in relation to the wavenumber. After this, the data was subjected to a Fourier-transform and the result obtained. The type of plastic was then identified with the help of a software library. A PerkinElmer Spectrum Two spectrometer was operated in attenuated total reflectance (ATR) mode and the results given in percent transmittance.

Differential scanning calorimetry (DSC)

The DSC analysis of POE and EVA samples was carried out using a Setaram C80 D reaction calorimeter. The samples were weighed on a Mettler Toledo analytical scale before being placed into an aluminium foil sample holder and a standard stainless-steel measurement cell. Only the aluminium foil was used as a reference. Prior to taking measurements, the system was pre-heated to 30 °C (room temperature + 10 °C) at a rate of 0.1°C/min and maintained at that temperature for an additional 2.0 hours to establish a thermal equilibrium. The DSC measurements were performed at a low heating rate of 0.6 °C/min from 30 to 280 °C which is justified because of the need to examine within the polymerising range. The results were analysed using Calisto software version 1.076. Peak integration was conducted using a sigmoidal-tangent peak baseline. The degree of crystallinity (X_c%)

of samples of granulated PET waste was determined according to the following equation:

$$\chi_c(\%) = \frac{\Delta H_{mp}}{\Delta H_{100}} \times 100\% \quad (1),$$

where ΔH_{mp} denotes the specific enthalpy of the melting transition and ΔH_{100} the specific enthalpy of the melting transition of completely crystalline polyethylene (288 J/g).

Gel content test

The goal of this test was to determine the degree of polymerization of the binding foil. The sample was prepared by placing the raw foil between two layers of PTFE before laminating them as complete solar panels. The EVA and POE samples must be examined in different ways in accordance with the manufacturer's recommendations. In the case of the EVA sample, it is placed into a Soxhlet-extractor device and extracted over 24 hours with toluene (Sigma-Aldrich, 99.5%). The POE sample is extracted with xylene (Sigma-Aldrich, 99.5%) and simply submerged in the solvent at 100 °C for 12 hours. In both cases, the degree of polymerization or the crosslinking ratio was calculated according to the difference in mass, where the foil is measured in its raw form before the test and in its dried out form after. The degree of polymerization is obtained by dividing the mass of the final product by the mass of the raw material.

Climate chamber test

The goal of this test was to simulate the effects of the environment on the solar panels and predict how they might respond to these impacts by conducting a standardized climate chamber test in accordance with the standard IEC 61215-2:2021 (MSZ EN IEC 61215-2:2021). During the test, the solar panels were subjected to a temperature cycle which consisted of a cold (-40 °C) and a warm-humid (85 °C) phase. These phases were maintained for 10 minutes before being cooled or heated at a maximum temperature gradient of 100 °C/hour. One cycle lasted 6 hours. The panels were subjected to 5, 10, 16 and 20 cycles. A visual representation of the cycle is shown in *Figure 2*. For the test, a Climats EXCAL 5423 HA climate chamber was used [23]. The original goal was to gain data on the degradation of the cell with regard to the overall effects of the environment, which were simulated by the chamber. When the root cause was sought, it was found that even this test was sufficient to initiate the desired changes, rendering the design of a new measuring method such as a damp heat test unnecessary.

Electroluminescence (EL) test

The test visualized the degradation of the panels and loss of the actual active surface of the wafers. The test took into account the fact that all solar cells emit light when a voltage is applied across their terminals in the forward direction (electroluminescence) in the infrared domain of the electromagnetic spectrum which is easily recordable with a camera. The obtained image then showed the active surface of the wafer as brighter areas, while the inactive, non-conducting parts remained dark.

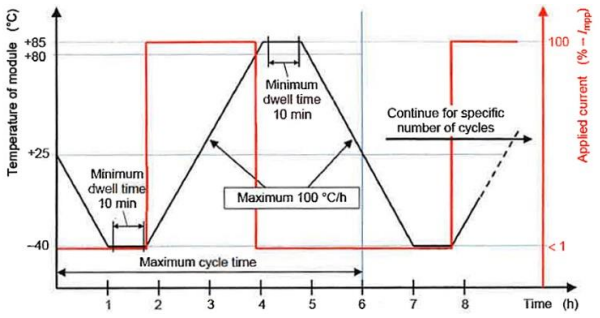

Figure 2: Thermal cycle diagram according to IEC 61215-2 [23]

Flash test

Multiple methods are available to test the power produced by solar panels. One of the quicker methods is the flash test where a predetermined, sudden flux of light was applied to the surface of the panel while the electrical output was connected to a changing artificial load and power meter. The maximum power output of the solar panel was then calculated from the measured electrical parameters. The measuring station was custom built and the light source an Ecoprogetti Ecosun Plus LED panel-type flashing lamp that was separated from the panel by a glass surface onto which the tested sample had to be placed wafer down. The outputs were connected to an ITECH IT8813-type load.

Corrosion model test

To simulate the effects of acetic acid on the strings of the solar panel, a corrosion model test was utilized. In this test, 1 and 10 vol.% solutions of the acid (diluted from a Sigma-Aldrich 20 vol.% solution) acted as corrosives. The test samples were pieces of ready-to-integrate strings sourced directly from the manufacturing line which were submerged in the solutions and left in closed containers at room temperature for a week. After this, the samples were washed with distilled water before being dried and visually evaluated by light and electron microscopy methods to simulate the results of long periods of operation in the field. While it would have been better to examine whole panels, the panels cannot be disassembled without directly damaging the components, leading to false results.

Microstructural examination using scanning electron microscopy (SEM)

Observations using a FEI/Thermo Fisher Apreo S SEM were conducted under high-vacuum conditions with an accelerating voltage of 20.0 kV. The samples were washed in an ultrasonic bath using ethanol and acetone before the backscattered images were taken and the chemical composition determined by an EDAX/Ametek Octane Elect Plus.

3. Results and discussion

During the work, two different material systems were used as the encapsulation foil. The first was a solar-grade EVA foil, while the other was a 'thermoplastic solar grade polyolefin' system, both are available commercially. During their manufacture, the parameters and methods recommended by the manufacturers were followed.

First, the exact chemical composition was determined using FTIR spectroscopy. In these tests, samples from the raw foil taken before the laminating process were examined. A comparison of the spectra can be found in *Figure 3*, where the spectrum of the EVA is colored pink and that of the POE blue. For the pink spectrum, the major transmittance valleys appeared at wavenumbers of 2917 (C-H), 2850 (C-H), 1737 (C=O), 1466 (C-H, methylene group), 1370 (C-H, methyl group), 1220 (C-O, vinyl ether), 1019 (C-O, vinyl ether) and 718 (C=C, cis-type alkene) cm^{-1}. These peaks and intensity ratios correspond to a copolymer which consists of 28 wt.% polyvinyl acetate and 72 wt.% polyethylene [18].

The blue spectrum consisted of less major transmittance valleys which appeared at wavenumbers of 2917 (C-H), 2850 (C-H), 1462 (C-H, methylene group) as well as 719 (C=C, cis-type alkene) cm^{-1} and can be attributed to the thermoplastic polyethylene [24]. However, other minor peaks were also present, suggesting the presence of additives or impurities in the foil. These peaks appeared at wavenumbers of 2932 (C-H, alkane), 1634 (N=O, secondary amine), 1536 and 679 (C=C, alkene) cm^{-1}. According to the Database of ATR-FT-IR spectra of various materials [25], these wavenumbers correspond to polyamide Nylon 6 which are significantly smaller than those of polyethylene, meaning that it is mostly composed of polyethylene with a small amount of Nylon 6. These results are in accordance with information provided by the supplier about them.

Table 2: The obtained data from the DSC measurements of the EVA and POE samples

EVA				
Peak	Onset (°C)	Peak max (°C)	Offset (°C)	Heat (J/g)
1 SMT	38.5	48.4	-	16.1
2 PMT	-	73.7	86.1	23.7
3 CT	123.3	127.3	157.5	-9.2
4 EOD	202.7	214.4	228.1	-29.0
POE				
Peak	Onset (°C)	Peak max (°C)	Offset (°C)	Heat (J/g)
1 SMT	36.7	45.9	-	15.4
2 PMT	-	68.5	78.5	13.2
3 CT	117.9	137.1	151.4	-12.9
4 EOD	171.3	208.7	260.6	-65.2

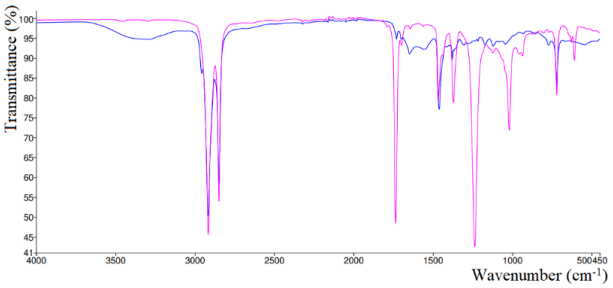

Figure 3: FTIR spectra of EVA (pink) and POE (blue)

The DSC data analysis of both POE and EVA samples shows distinct differences. POE resulted in secondary and primary melting transitions occurring at lower temperatures along with reduced levels of thermal absorption compared to the EVA sample. In addition, POE exhibits lower onset and offset temperatures. The calculated degree of crystallinity for the secondary melting transition was 5.60% for POE and 5.35% for EVA, while for the primary melting transition it was 8.21% for POE and 4.58% for EVA.

The measured DSC curves of the POE and EVA samples are shown in *Figure 4* with the obtained data presented in *Table 2*.

These values fall within the range of degree of crystallinity reported in the literature for uncured polymers. Both samples exhibited wide and segmented exothermic crosslinking transitions. In the case of POE, the peak took on a fronting shape with lower onset and offset temperatures but a higher peak maximum during the second reaction phase. Conversely, EVA displayed a tailing shape peak with higher onset and offset temperatures but a lower peak maximum during the first phase of the reaction. The exothermic oxidation peak of POE began at a significantly lower temperature compared to that of EVA where more heat was released [26]-[28].

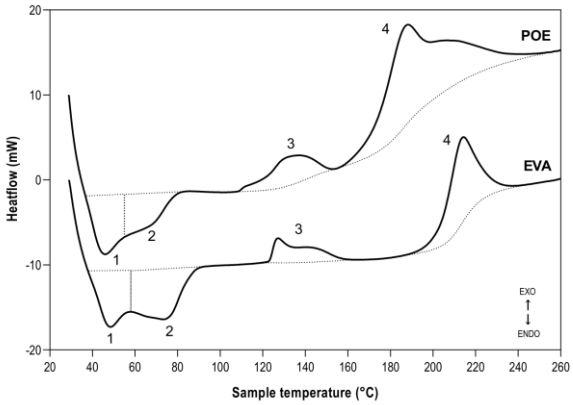

Figure 4: DSC curves of POE and EVA samples over a heating range from 30 to 280 °C (heating rate: 0.6 °C/min)
1 = Secondary melting transition (SMT)
2 = Primary melting transition (PMT)
3 = Crosslinking transition (CT)
4 = Exothermic oxidation / degradation (EOD)

Table 3: Degree of polymerization of the different encapsulating agents

	Gel content (%)	AV	SD
EVA_1	86.50		
EVA_2	83.40	84.70	1.61
EVA_3	84.20		
POE_1	66.27		
POE_2	65.16	66.25	1.08
POE_3	67.32		

AV: average of the measured values, SD: standard deviation of the measured values

Table 4: The electrical parameters of panels manufactured with different foils after a certain number of thermal cycles.

	Isc (A)	*Voc* (V)	*Ipm* (A)	*Vpm* (V)	*Pm* (W)
EVA_0	0.263	51.401	0.224	43.022	9.637
EVA_5	0.264	51.259	0.225	42.888	9.652
EVA_10	0.263	51.620	0.224	42.038	9.408
EVA_16	0.262	51.375	0.200	39.515	7.902
EVA_20	0.263	50.875	0.197	34.845	6.865
POE_0	0.260	51.077	0.233	43.647	10.152
POE_5	0.261	50.942	0.232	43.623	10.133
POE_10	0.262	51.146	0.237	43.239	10.238
POE_16	0.260	50.956	0.235	42.983	10.117
POE_20	0.261	50.599	0.235	42.626	10.015

Isc: short circuit current, *Voc*: the open circuit voltage, *Ipm*: the current, *Vpm*: voltage at the maximum power point, *Pm*: maximum power

The degree of polymerization is an important quality of solar panels which shows how much of the plastic has polymerized as well as what proportion remained in oligomeric and monomeric forms. It must closely resemble the percentage given by the manufacturer of the foil at which the encapsulation foil exhibits optimal properties.

During the experiments, the laminator was always set up according to the foil's manufacturer's recommendations to ensure that the mechanical properties of and imperfections in the foils did not distort the results of the climate chamber tests. Measurements were also taken according to the preferred and official methods stated by the manufacturer. For the EVA foil, Soxhlet-extraction with toluene for 24 hours was performed. The POE foil was immersed in xylene and kept at 100 °C for 12 hours. Samples were taken by cutting off a piece of the raw foil, measuring its weight, layering it between two strips of PTFE and feeding it into the laminator as if it were to become a solar panel. Having cooled down, the extraction processes were performed and the samples dried before measuring their weights. The determined crosslinking ratio or gel content of these samples can be found in *Table 3*, where AV denotes the average of these measurements and SD their standard deviation. It was found that all the foils closely resembled the optimal degree of polymerization based on the manufacturer's recommendations, that is, 85 wt.% for the EVA foil and 66 wt.% for the POE foil. As a result, these foils are not likely to suffer mechanical failures and provide a good basis for comparisons.

While it would have been better to have the plastics examined directly from the manufactured solar panels, the plastic encapsulant cannot be removed from the laminate without damaging the materials in question, falsifying the results. As a result, the PTFE foils were used instead. In addition, the initial mass was not measurable directly. While the weight of the individual raw foil could be measured, a considerable amount of plastic was lost in the lamination process, which was removed as excess foil. This waste product also yielded false results as the backsheet and the EVA/POE foil were mixed in it, falsifying any measurements.

During the research, all the solar panel specimens were subjected to a climate chamber test. The thermal cycle and other test conditions were established according to the IEC 61215-2 standard. After a given number of cycles, the panels were taken out of the chamber before measurements were taken on them. To examine the degrading effects of the weather on the panels, a flash test was conducted from which the main parameters for determining the operating conditions of the solar panels were obtainable, namely the short circuit current (*Isc*), the open circuit voltage (*Voc*) as well as the current (*Ipm*) and voltage (*Vpm*) at the maximum power point. From these values, the maximum power of the panels could be calculated. These measured parameters can be found in *Table 4*. The measurements were taken before the test as well as after 5, 10, 16 and 20 cycles. The maximum output power of the measurements as a function of the number of thermal cycles the panels were subjected to is shown in *Figure 5*. Although it is clearly observable that both types degrade over time, the rate of this degradation varies. The samples made with EVA foil denoted in red exhibited accelerated power loss between the 10th and 20th cycles amounting to a reduction in the maximum power of around 30%. The solar panels made with POE denoted in black were much more resistant as their power loss fell within the margin of the measurement error.

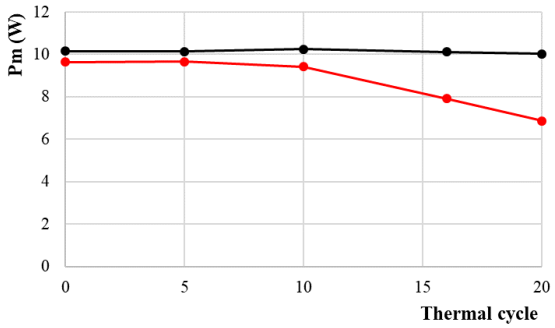

Figure 5: The performance of solar panels manufactured with EVA (red) and POE (black) as a function of the number of cycles in climate chamber tests

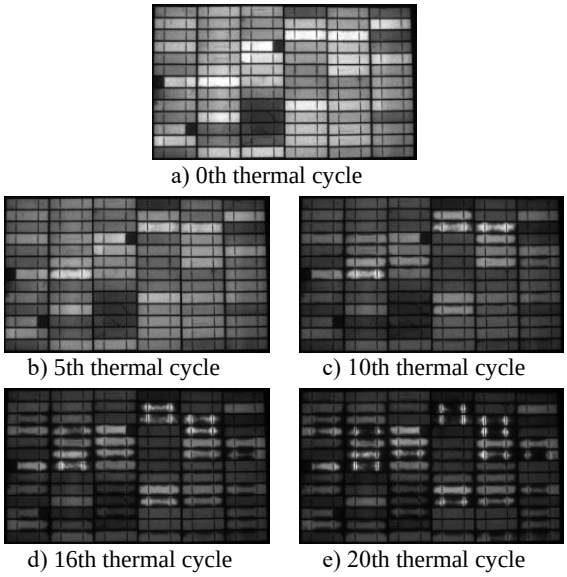

Figure 6: Electroluminescence images of the EVA-based panels after a certain number of thermal cycles

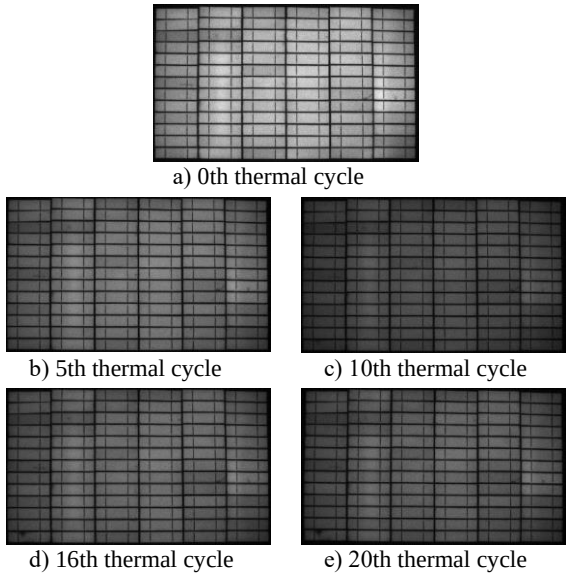

Figure 7: Electroluminescence images of the POE-based panels after a certain number of thermal cycles

After every power measurement, the panels were subjected to an EL test to visually observe the degradation of the conductive parts. The images of the panels made with EVA are presented in *Figure 6* in which only the most prominent series are shown.

These images clearly show an advanced degree of degradation since the wafers got progressively darker as the number of cycles increased. However, a more concerning sign of degradation was the uneven level of luminescence of the wafers. Even in *Figure 6b* after 5 thermal cycles, some wafers only emitted light from areas near to the external conducting material. This effect becomes more prominent as the number of cycles increases. The darkening pattern suggests increased series resistance, perhaps originating from microstructural changes in the ribbons, caused by corrosion.

On the other hand, according to *Figure 7*, the alternative material is promising from corrosion and degradation points of view as the darkening effect is not visible, only a slight change in brightness. This suggests that the corrosion is induced by the acetic acid originating from the decomposition of EVA.

The EL test results are further supported by the flash test. Here, the series resistance of the modules made with EVA in some cases even tripled after 20 cycles, whereas only a minor change was observable in the other group. This lead to the tendency shown in *Figure 8* where the two types of panels initially responded equally, however, as the test progressed, the rate of degradation of the EVA cells increased and their maximum power deteriorated drastically. In one case after 20 cycles, the output power of the cell dropped by 40% compared to at the beginning of the test. In the case of the POE-based material, this change was not prominent since the largest reduction was around 10%.

To simulate the effects of the decomposing EVA foil, a corrosion model test was performed where solutions of acetic acid were prepared at concentrations

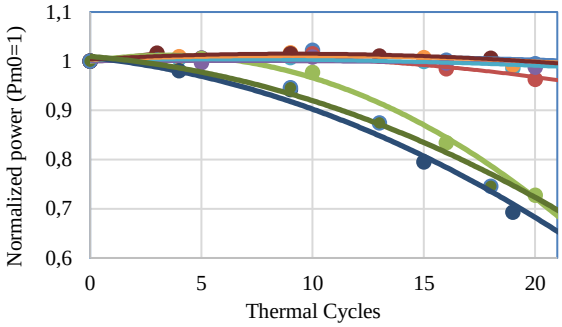

Figure 8: The normalized power of the cells in relation to the number of thermal cycles

of 1 and 10 vol.%. The samples, which were ready-to-integrate pieces of string, were immersed in these solutions for one week before being washed and dried samples examined then compared visually to their initial state and with SEM methods. During the instrumental analysis, an attempt was made to reproduce all the initial images. While the measurements are over-representative with regard to the stresses the material is actually subjected to over 20 thermal cycles, the goal here was to create a test where the effects of the acid could be examined relatively quickly.

Degradation was confirmed visually. The backside of the wafers was shiny, compared to its initial matte finish. The thin busbars, which run along the surface of the wafers, were damaged. In both cases, one of the ribbons detached from the wafers.

The reason for the reduction in power shown in *Figure 6* can be explained by the SEM images shown in *Figure 9*. The pairs of images taken at low levels of magnification (*Figures 9a, 9c, 9e* and *9g*) show roughening of the surface of the ribbons proving that they had started to decay. In the higher magnification images (*Figures 9b, 9d, 9f* and *9h*), it can be seen that the acetic acid did not react equally with the materials the ribbon is

Table 5: Composition of the remaining crystals from the corrosion model test determined by EDS analysis

Element	Atomic %
C	26.59 ± 2.70
O	56.83 ± 4.76
Na	0.85 ± 0.18
Al	12.09 ± 0.71
Si	0.57 ± 0.09
Pb	0.05 ± 0.01
Cl	0.20 ± 0.04
Sn	2.87 ± 0.13

composed of and consumed the darker-colored areas. As the imaging method is based on the detection of backscattered electrons (BSE), the lighter areas and/or pixels represent elements with lower atomic numbers, e.g. tin (Sn), detrimentally affecting the mechanical stability of the ribbons as the reduction in tin content may cause these parts to break. In addition, the series resistance increased, increasing power loss from the solar panel. Darkening of almost the whole of the affected wafers can be explained by the breaking of the busbars.

After the corrosion model test, the remaining acetic acid solution was evaporated and the remaining powder sample analyzed by SEM using the EDS detector. The spectra recorded suggest the composition shown in *Table 5*.

The high carbon content and the almost twice as large oxygen content suggested that the powder was some kind of acetate salt. The high aluminum content explains why the backside of the wafers became shiny, namely they were completely corroded by the acetic acid. The aluminum may have also originated from the ribbon as a component of a combined metal. The selective consumption of the ribbon was also observable here since the tin content of the recovered crystals was much higher than their lead content. In fact, the lead content of the sample was just barely higher than the background noise of the detector, rendering it hardly detectable.

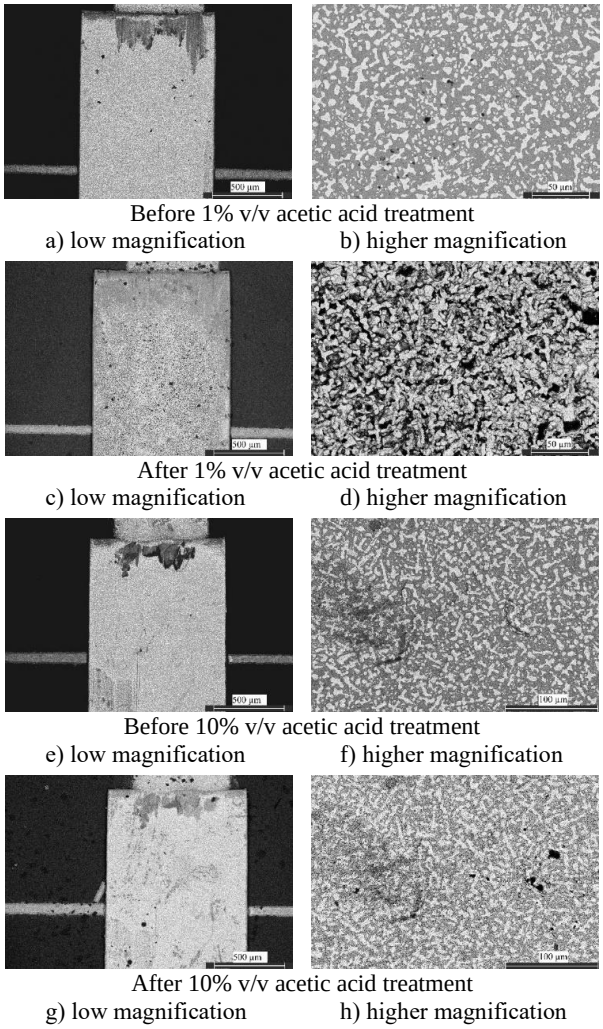

Before 1% v/v acetic acid treatment
a) low magnification b) higher magnification

After 1% v/v acetic acid treatment
c) low magnification d) higher magnification

Before 10% v/v acetic acid treatment
e) low magnification f) higher magnification

After 10% v/v acetic acid treatment
g) low magnification h) higher magnification

Figure 9: SEM images of the wafers before and after the corrosion model tests
(The images were captured by a BSE detector.)

4. Conclusions

In this article, the causes and effects of the decomposition of EVA foil in solar panels were examined as well as discussed. The effects of the corrosion agent were simulated and the results compared before and after. An alternative material based on polyethylene was also examined and a series of solar panels containing it was subjected to the same standardized accelerated aging tests as the ones equipped with EVA.

The experimental results clearly show that acetic acid corrosion causes severe irreversible damage to the electrical components of solar cells preventing much of each wafer from producing electricity. As this detrimental effect did not occur when the other polyethylene-based foil was used, it can be stated that this foil is a promising alternative to the classical EVA foil. While the manufacturer's datasheet states that the properties of the final product should be identical to one made with EVA, an intensive life-cycle test amongst other tests (mechanical, chemical resistance tests, etc.) would be required to verify this claim.

Acknowledgements

The research was supported by the ÚNKP-23-1 New National Excellence Programme of the Ministry for Innovation and Technology financed by the National Research, Development and Innovation Fund.

The GINOP_Plusz-2.1.1-21-2022-00225 project was implemented with the support of the Ministry for Innovation and Technology through the National Research, Development and Innovation Fund.

REFERENCES

[1] Energy statistics data browser – Data tools – IEA https://www.iea.org/data-and-statistics/data-tools/energy-statistics-data-browser?country=WORLD&fuel=Energy%20supply&indicator=ElecGenByFuel (accessed 2023.10.22.)

[2] Gergely, A., Kristóf, T.: Corrosion protection with ultrathin graphene coatings: a review, *Hung. J. Ind. Chem.*, 2013, **41**(2), 83–108, DOI: 10.1515/508

[3] Köntges, M.; Oreski, G.; Jahn, U.; Herz, M.; Hacke, P.; Weiss, K.-A.; Razongles, G.; Paggi, M.; Parlevliet, D.; Tanahashi, T.; French, R.H.; Richter, M.; Tjengdrawira, C.; Morlier, A.; Li, H.; Perret-Aebi, L.-E.; Berger, K.A.; Makrides, G.; Herrmann, W.: Assessment of photovoltaic module failures in the field (Report IEA-PVPS T13-09:2017) (IEA, Paris, France), 2017, ISBN: 9783906042541

[4] Pingel, S.; Frank, O.; Winkler, M.; Oaryan, S.; Geipel, T.; Hoehne, H.; Berghold, J.: Potential induced degradation of solar cells and panels, *Proc. 35th IEEE Photovolt. Spec. Conf., Honolulu, HI, USA*, 2010, 2817–2822, DOI: 10.1109/PVSC.2010.5616823

[5] Aghaei, M.; Fairbrother, A.; Gok, A.; Ahmad, S.; Kazim, S.; Lobato, K.; Oreski, G.; Reinders, A.; Schmitz, J.; Theelen, M.; Yilmaz, P.; Kettle, J.: Review of degradation and failure phenomena in photovoltaic modules, *Renew. Sustain. Energy Rev.*, 2022, **159**, 112160, DOI: 10.1016/j.rser.2022.112160

[6] Hasan, A.A.Q.; Alkahtani, A.A.; Shahahmadi, S.A.; Alam, M.N.E.; Islam, M.A.; Amin, N.: Delamination-and electromigration-related failures in solar panels - a review, *Sustainability*, 2021, **13**(12), 6882, DOI: 10.3390/su13126882

[7] Schnatmann, A.K.; Schoden, F.; Schwenzfeier-Hellkamp, E.: Sustainable PV module design - review of state-of-the-art encapsulation methods, *Sustainability*, 2022, **14**(16), 9971, DOI: 10.3390/su14169971

[8] El-Garabawhi, A.A.S.A.: Review on corrosion in solar panels, *Int. J. Smart Grid*, 2018, **2**(4), 218–220, DOI: 10.20508/ijsmartgrid.v2i4.31.g29

[9] de Oliveira, M.C.C.; Diniz Cardoso, A.S.A.; Viana, M.M.; Lins, V.D.F.C.: The causes and effects of degradation of encapsulant ethylene vinyl acetate copolymer (EVA) in crystalline silicon photovoltaic modules: A review, *Renew. Sustain. Energy Rev.*, 2018, **81**, 2299–2317, DOI: 10.1016/j.rser.2017.06.039

[10] Marín, M.L.; Jiménez, A.; López J.; Vilaplana, J.: Thermal degradation of ethylene (vinyl acetate). Kinetic analysis of thermogravimetric data, *J. Therm. Anal.*, 1996, **47**(1), 247–258, DOI: 10.1007/BF01982703

[11] Weber, U.; Eiden, R.; Strubel, C.; Sögding, T.; Heiss, M.; Zachmann, P.; Nattermann, K.; Engelmann, H.; Dethlefsen, A.; Lenck, N.: Acetic acid production, migration and corrosion effects in ethylene-vinyl-acetate- (EVA-) based PV modules, *Proc. 27th EU PVSEC, Frankfurt, Germany*, 2012, 2992–2995, DOI: 10.4229/27thEUPVSEC2012-4CO.9.4

[12] Semba, T.; Shimada, T.; Shirasawa, K.Y.K.; Takato, H.: Corrosion of the glass and formation of lead compounds in the metallization by high temperature and high humidity test of crystalline silicon PV module, *Proc. 2018 IEEE 7th WCPEC, Waikoloa, HI, USA*, 2018, 1333–1335, DOI: 10.1109/pvsc.2018.8548005

[13] Semba, T.: Corrosion mechanism analysis of the front-side metallization of a crystalline silicon PV module by a high-temperature and high-humidity test, *Jpn. J. Appl. Phys.*, 2020, **59**(5), 054001, DOI: 10.35848/1347-4065/ab8274

[14] Gaddam, S.K.; Pothu, R.; Boddula, R.: Advanced polymer encapsulates for photovoltaic devices − A review, *J. Mater.*, 2021, **7**(5), 920–928, DOI: 10.1016/j.jmat.2021.04.004

[15] Czanderna, A.W.; Pern, F.J.: Encapsulation of PV modules using ethylene vinyl acetate copolymer as a pottant: A critical review, *Sol. Energy Mater. Sol. Cells*, 1996, **43**(2), 101–181, DOI: 10.1016/0927-0248(95)00150-6

[16] Miller, L.L.; Bernstein, R.; White II, G.V.; Schroeder, J.L.; Hochrein, J.M.: Acetic acid as a degradation product or inventory of ethylene-vinyl acetate (EVA) (Presentation), *JOWOG 2013, AWE, Aldermaston, UK*, 2013

[17] López-Escalante, M.C.; Caballero, L.J.; Martín, F.; Gabás, M.; Cuevas, A.; Ramos-Barrado, J.R.: Polyolefin as PID-resistant encapsulant material in PV modules, *Sol. Energy Mater. Sol. Cells*, 2016, **144**, 691–699, DOI: 10.1016/j.solmat.2015.10.009

[18] Ottersböck, B.; Oreski, G.; Pinter, G.: Comparison of different microclimate effects on the aging behavior of encapsulation materials used in photovoltaic modules, *Polym. Degrad. Stab.*, 2017, **138**, 182–191, DOI: 10.1016/j.polymdegradstab.2017.03.010

[19] Oreski, G.; Omazic, A.; Eder, G.C.; Voronko, Y.; Neumaier, L.; Mühleisen, W.; Hirschl, C.; Ujvari, G.; Ebner, R.; Edler, M.: Properties and degradation behavior of polyolefin encapsulants for photovoltaic modules, *Prog. Photovolt. Res. Appl.*, 2020, **28**(12), 1277–1288, DOI: 10.1002/pip.3323

[20] Adothu, B.; Bhatt, P.; Chattopadhyay, S.; Zele, S.; Oderkerk, J.; Sagar, H.P.; Costa, F.R.; Mallick, S.: Newly developed thermoplastic polyolefin encapsulant–A potential candidate for crystalline silicon photovoltaic modules encapsulation, *Sol. Energy*, 2019, **194**, 581–588, DOI: 10.1016/j.solener.2019.11.018

[21] J. Woghlemuth.: Introduction: Group #3: Humidity, Temperature and Voltage, In: *PVRW*, Lakewood, CO, USA, 2013

[22] K. Withfeld and A. Salomon: Modeling based on Damp Heat Testing (2012) https://www1.eere.energy.gov/solar//pdfs/pvmrw12_tuespm_solaria_whitfield.pdf (accessed on 2023.12.15.)

[23] Standard IEC 61215-2:2021 (MSZ EN IEC 61215-2:2021): Terrestrial photovoltaic (PV) modules - Design qualification and type approval - Part 2: Test procedures

[24] Barretta, C.; Oreski, G.; Feldbacher, S.; Resch-Fauster, K.; Pantani, R.: Comparison of degradation behavior of newly developed encapsulation materials for photovoltaic applications under different artificial ageing tests, *Polymers*, 2021, **13**(2), 271, DOI: 10.3390/polym13020271

[25] Polyamide (Nylon 6) – Database of ATR-FT-IR spectra of various materials https://spectra.chem.ut.ee/textile-fibres/polyamide/ (accessed on 2023.12.10.)

[26] Adothu, B.; Bhatt, P.; Kartikay, P.; Zele, S.; Costa, F.R.; Oderkerk, J.; Mallick, S.: Determination of crystallinity and thermal stability of newly developed thermoplastic polyolefin encapsulant for the c-Si PV module application, *Proc. 2019 IEEE 46th Photovolt. Spec. Conf., Chicago, IL, USA*, 2019, 487–490, DOI: 10.1109/pvsc40753.2019.8980526

[27] Adothu, B.; Mallick, S.; Kartikay, P.: Determination of crystallinity, composition, and thermal stability of ethylene vinyl acetate encapsulant used for PV module lamination, *Proc. 2019 IEEE 46th Photovolt. Spec. Conf., Chicago, IL, USA*, 2019, 491–494, DOI: 10.1109/pvsc40753.2019.8981151

[28] Agroui, K.; Collins, G.: Determination of thermal properties of crosslinked EVA encapsulant material in outdoor exposure by TSC and DSC methods, *Renew. Energy*, 2014, **63**, 741–746, DOI: 10.1016/j.renene.2013.10.013